Deformation-Induced Morphology Changes and Orientation Behavior in Syndiotactic Polypropylene

Michael S. Sevegney, Gautam Parthasarthy, and Rangaramanujam M. Kannan*

Department of Chemical Engineering and Materials Science, Wayne State University, Detroit, Michigan 48202

Derek W. Thurman and Lucia Fernandez-Ballester

Division of Chemistry and Chemical Engineering, California Institute of Technology, Pasadena, California 91125

Received October 24, 2002; Revised Manuscript Received May 21, 2003

ABSTRACT: Syndiotactic polypropylene (sPP) exhibits a complex crystalline morphology, characterized by unique annealing- and deformation-induced changes. Rheooptical FTIR spectroscopy, wide-angle X-ray diffraction (WAXD), and Raman spectroscopy are used to characterize morphology and orientation responses of highly syndiotactic sPP to tensile drawing. Solid-state thin films of different initial morphology, either quenched or slowly cooled from the melt, are studied. Results suggest that a gradual transition in macromolecular chain conformation, from gauche−gauche−trans−trans helical to all-trans planar, is observed at room temperature for quenched samples that are drawn up to 400% strain. This transition is marked initially by the gradual disappearance of helical chains (disordered form I) and the subsequent emergence of a mesophase, which may transform into form III crystals at even greater strains. Our primary investigational tool, the rheo-FTIR spectrometer, allows us to monitor the presence and orientation of amorphous, mesomorphic, and crystalline domains directly, simultaneously, and sensitively. Results from all of the techniques used are correlated in an effort both to assign IR peaks to characteristic sPP moieties and to generate a plausible physical model of the deformation dynamics in melt-quenched sPP.

Introduction and Background

Recent developments in metallocene catalysts have made it possible to tailor the tacticity of polypropylene.[1−3] Isotactic polypropylene (iPP) is a highly crystalline, "high-strength" material whereas syndiotactic polypropylene (sPP) is less crystalline, more ductile at room temperature, and possesses greater impact strength and a lower entanglement molecular weight.[4,5] Metallocene-catalyzed, highly stereoregular sPP can be an elastomeric alternative to iPP for some applications, without radical differences in thermal properties.[6] Additionally, sPP might have strong potential as a blending component with its atactic and isotactic counterparts.[7,8] sPP has also been found to resist oxidative degradation to a greater degree than iPP.[9,10] The complex polymorphism of sPP has presented an interesting challenge in attempting to understand its structure−property relationships.

To date, four crystalline structures of sPP have been identified. Each is composed primarily of macromolecular chains adopting a gauche−gauche-trans−trans $(ggtt)_n$ helix conformation, an all-trans $(tttt)_n$ planar conformation, or sequential blocks of each conformation. The most stable (and, by far, best-understood) crystalline morphology, commonly known as form I, was first identified by Lotz, Lovinger, and co-workers.[11,12] Form I is composed of helical chains packed in an orthorhombic lattice with parameters $a = 14.50$ Å, $b = 11.20$ Å, and $c = 7.45$ Å (space group *Ibca*). The chain axis is coincident with the *c* axis, and chains adopt a fully antichiral packing order (i.e., adjacent chains are of alternating handedness along both the *a* axis and *b* axis). This form has been obtained most readily by slowly crystallizing highly syndiotactic material from the melt at elevated temperatures.[13,14] When crystallized at lower temperatures (generally below 120 °C), intermolecular packing disorders along the *b* axis are introduced, and a helical crystal modification, with lattice parameters $a = 14.50$ Å, $b = 5.60$ Å, and $c = 7.45$ Å (space group *Pcaa*), may be obtained.[13,14] Form II, the *c*-centered analogue of form I, also has an orthorhombic crystal structure with parameters identical to the disordered form I ($a = 14.50$ Å, $b = 5.60$ Å, and $c = 7.45$ Å). In this modification, however, helices of like handedness are adjacent to one another along both the *a* axis and *b* axis (space group $C222_1$). Understandably, crystallographic analysis of sPP must be performed very carefully in order to determine the presence of either a limit-ordered or a disordered crystal modification. Fortunately, the literature contains several rigorous analyses of both electron[11−13] and X-ray[15−18] diffraction results that distinguish unequivocally one helical crystal modification from another. In general, form II is obtained more readily from sPP of lower stereoregular content.[18] Form II also has been obtained by precipitating sPP from its polymerization medium,[17,19] by epitaxial crystallization on an appropriate surface,[20] by tensile drawing films of low stereoregularity,[15,18] and by either annealing[15] or releasing from tension[18,21,22] films of high stereoregularity that were slowly melt-crystallized (i.e., initially rich in form I) and subsequently tensile drawn. Crystalline form III is a

* To whom correspondence should be addressed: E-mail: rkannan@che.eng.wayne.edu.

10.1021/ma025774+ CCC: $25.00
Published on Web 07/22/2003

metastable sPP polymorph composed of all-trans-planar zigzag chains in an orthorhombic unit cell of lattice parameters $a = 5.22$ Å, $b = 11.17$ Å, and $c = 5.06$ Å.[23,24] Initially, Chatani et al. observed form III in sPP films that were quenched from the melt and subsequently tensile drawn (all at 0 °C).[25] Similar results have been obtained by others for melt-quenched films,[21,26−30] melt-crystallized films,[18,22] and melt-spun fibers[31] that are subjected to high tensile strains (≥400%) at different temperatures. Nakaoki et al. claim the spontaneous, though very slow, formation of form III when ice−water-quenched samples are left at 0 °C for a considerable amount of time (∼2 months).[32,33] In fact, this is the only report of form III appearing in the absence of some applied mechanical stress. The identification of "cold-crystallized" form III remains a topic for discussion.[34] Form IV, the least well-known of the four crystalline structures, is composed of chains adopting a $(ttttttggttgg)_n$ conformation, arranged in a triclinic unit cell with lattice parameters $a = 5.72$ Å, $b = 7.64$ Å, $c = 11.60$ Å, $\alpha = 73.1°$, $\beta = 88.8°$, and $\gamma = 112.0°$.[35,36] Chatani et al. first obtained this polymorph upon exposing quenched cold drawn sPP films (rich in form III) to appropriate solvent vapors (benzene, toluene, or *p*-xylene) for several days.[35] When annealed above 50 °C (for sufficient time), sPP will revert to the most thermodynamically stable form, form I.[15,18,34,35]

Sufficiently thick films and fibers of sPP have exhibited highly elastomeric behavior during tensile mechanical testing.[21,22,30,31] This behavior seems to be present without regard to sample preparation conditions. Deformation-induced morphology changes are thought to be responsible for elasticity. De Rosa and co-workers have demonstrated this for room-temperature-quenched[21] and melt-slow-cooled[22] undeformed films, which are rich in form I crystals. At strains much greater than 400%, the films are rich in form III crystals. This observation suggests a change in overall chain conformation (from helical to planar zigzag) had to occur. Upon release of tension, the films return primarily to helical crystalline states (form I or II, depending on the stretching conditions[22]). De Rosa et al. suggest that the crystal−crystal transformation observed is a strong enthalpic contribution to the overall energetics that drive this elastic behavior. However, they concede that entropic forces originating from the relaxation of highly oriented amorphous chains (as observed in traditional thermoplastic elastomers) may also contribute.

Alternatively, Guadagno et al. have investigated elastomeric behavior for melt-quenched sPP films, which are initially rich in trans-planar chains.[29,30] These films also contain form III crystals while under tension (strain ≥ 600%) at room temperature.[29] Unlike slowly cooled films, however, these melt-quenched films revert mostly to planar chains upon release of tension. Some helical chains do appear also, but to a much lesser extent. Cold drawing these films and maintaining tension at low temperature cause helical chains to be entirely absent upon film relaxation.[30] Thus, elastomeric behavior is also observed for melt-quenched, tensile deformed sPP, but without a crystal−crystal transformation. (In fact, the results of ref 30 do not show even a change in chain conformation.) X-ray diffraction,[25,34] thermal and mechanical analyses[27] of melt-quenched sPP suggest that the planar chains formed initially do not compose an entangled amorphous domain. Instead, it is thought that planar chains exist as a loosely aggregated, paracrystalline domain (or "mesophase", so named by Vittoria et al.[34]). This mesophase may act as a physical cross-linking agent, thus imparting mechanical and thermal properties quite different than those of an entangled amorphous material.[27,37,38]

In this work, we use a combination of mechanical, X-ray diffraction, infrared and Raman spectroscopic techniques to address deformation-induced structural changes and orientation and relaxation behavior of this complex semicrystalline polymer. We will also illustrate the abilities of our recently developed rheo-FTIR spectrometer[39] to measure molecular orientation in crystalline, mesoscopic, and amorphous domains quantitatively, sensitively, and simultaneously. This is achieved by measuring the infrared linear dichroism (IRLD) *spectra* of solid-state thin films subjected to irreversible tensile strain. Our experimental strategy is unique in the sense that both morphology and orientation behavior will be observed directly as thin sPP films are stretched up to and beyond the yield point. Over this region of tensile strains, the gradual change in chain conformation is observed clearly, as are the orientation responses of helical and planar chains to the applied strain. Results from the various techniques used illustrate the deformation-induced "path" traversed by sPP from a morphology initially rich in form I helical crystals to a planar rich mesomorphic stage, which is a precursor to the appearance of form III.

Experimental Section

Materials. Highly syndiotactic polypropylene (∼90% *r*) was obtained from the Fina Oil and Chemical Company (Dallas, TX). Weight- and number-averaged molecular weights were determined via high-temperature size exclusion chromatography to be 228 500 and 60 600, respectively, based on polystyrene standards. Thin films (≈100 μm) were formed by compression molding (Hydraulic Unit model 3912, Carver, Inc.) the melt between acetone-cleaned glass slides. Solid sPP pellets (as received from Fina) were heated to 177 °C (350 °F) and held for 20 min, allowing the sample to melt thoroughly. A second clean glass slide is then placed on top of the melt, covering it, and the ensemble is pressed so as to form a film of nearly uniform thickness. Upon molding the film, the pressing load is removed and the film is allowed to anneal at 177 °C for 30 min. This step is performed in order to remove any residual molecular orientation imposed on the sample by melt pressing. At this point, sample preparation is completed in one of two ways, depending on the initial morphology desired in the solid-state film.

1. To achieve a sample that contains almost exclusively helical chain conformation and is rich in form I crystallites, the sample is slowly cooled to room temperature (∼30 °C). This is achieved simply by leaving the sample between the press blocks and deactivating their heating elements. Room temperature is reached in approximately 4 h. "Slow-cooled" samples are stored at room temperature until used.

2. Alternatively, we may form films of much lower crystalline content and richer in planar molecular chains. To do this, the sample is directly quenched into liquid nitrogen (∼−170 °C), thereby arresting the formation of any crystalline domains of appreciable size. These "quenched" samples are stored below the glass transition temperature ($T = -10$ °C $< T_g \approx 0$ °C) until they are used in experiments. Quenched samples are allowed to equilibrate at room temperature for about 30 min before rheo-FTIR experiments are performed. This equilibration step is thought to be responsible for the initial presence of form I crystals in our samples.

Solid sample films are easily removed from between the glass slides by gently prying the slides apart with a straight razor blade. Gauge samples are then cut from solid films in

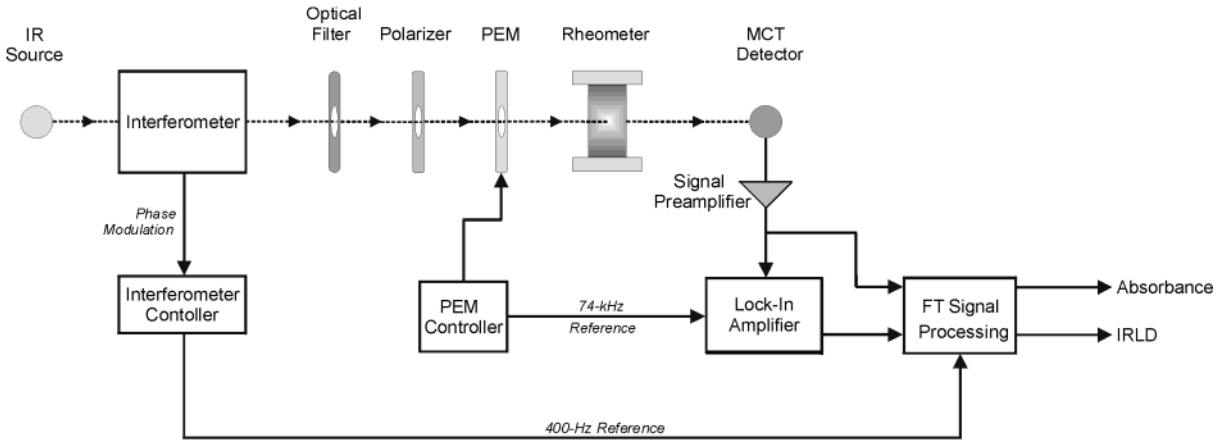

Figure 1. Schematic diagram of the rheo-FTIR spectrometer optical and signal processing trains. Optical and electric signals are represented by dashed and solid lines, respectively.

the mechanical press at room temperature using a steel die tool of rectangular geometry (14.7 mm × 5.61 mm). Last, gauge thickness is measured prior to stretching. It is important to note here the difficulty involved not only in molding films of uniform thickness, but also in achieving the same sample thickness over repeated sample preparations. Transmission mode IR spectroscopy requires that the sample gauge thickness be approximately 100 μm, so as to avoid peak saturation in the region of interest. To a certain extent, this limits the strain-to-failure values achieved during our experiments.

Methods. Rheo-FTIR Spectroscopy. We have developed a state-of-the-art instrument capable of measuring molecular orientation for both crystalline and amorphous domains within semicrystalline polymers.[39] Infrared linear dichroism (IRLD) spectra are measured, allowing us to quantify orientation behavior for many moieties simultaneously. Spectra can be acquired for samples as they undergo various degrees of tensile strain and at different temperatures. Additionally, infrared absorbance spectra can also be extracted from raw dichroism data. This feature allows us to monitor changes in sample morphology by observing intensity changes in conformation-sensitive IR peaks. The sections to follow provide a summary of equipment used in rheo-FTIR experiments. The optical and signal processing trains are similar to the apparatus developed by Fuller, but with a few key differences.[40]

FTIR Spectrometer. A Fourier transform infrared spectrometer (Bio-Rad model FTS 6000) is essentially used as a polychromatic mid-IR radiation source (wavelengths, $\lambda = 2.5$ to 25 μm or wavenumbers, $\tilde{\nu} = 4000$ to 400 cm^{-1}). It is capable of imposing interferometric modulation on the source light in both continuous-scan (i.e., "rapid-scan") and step-scan modes. This Michelson interferometer is AC coupled with a liquid-nitrogen-cooled fast mercury−cadmium−telluride (MCT) detector. Because of the nature of these experiments, it is necessary for the instrument to operate in step-scan mode. In conventional continuous-scan FTIR spectroscopy, the interferogram itself is time-dependent.[41] This makes detector signal processing very difficult, as the interferometric modulation may be indistinguishable from other time-dependent phenomena imposed upon the source light (e.g., dynamic sample perturbation, transience in the polarization state of source light). For IR experiments, the moving mirror undergoes a stepping motion at a frequency of 400 Hz (steps per second). This helps to label the source light, further distinguishing it from noise and stray background radiation. Using a plane mirror, the intensity-modulated source is directed through an external port into a custom-built external chamber. The beam is then further redirected, passed through a series of optical elements (optical low-pass filter, linear polarizer, photoelastic modulator, and sample chamber, successively), and focused onto a sample, where it is partially absorbed and then transmitted to the MCT detector. A diagram of this optical train is given as Figure 1.

Polarization Optics. Source light is passed through a wire-grid linear polarizer, which defines the reference axis (chosen to be parallel to the axis of uniaxial sample deformation). A photoelastic modulator (PEM-90/ZS37, zinc selenide crystal, Hinds Instruments, Inc.) is used to impose a high frequency, broadband polarization modulation in the midinfrared electromagnetic region. When its retardation amplitude is set to one-half wave, the PEM acts like a half-wave plate, rotating the incident beam plane of polarization by 90° at the PEM characteristic frequency ($\omega_{PEM} \approx 37$ kHz). More precisely, the IR beam alternates between two mutually perpendicular plane polarized states at a frequency of $2\omega_{PEM} \approx 74$ kHz. This is the frequency at which the desired IRLD signal can be detected. Of further note, the polarization modulation also serves as a "carrier" signal for the lower-frequency interferometer modulation. The PEM also improves the overall signal-to-noise ratio because of multiplicative noise suppression due to averaging.

Sample Chamber. A miniature materials tester (Minimat 2000, Rheometric Scientific, Inc.) is used to apply large, irreversible tensile deformation to sPP thin films. Samples are stretched stepwise in distinct increments at an elongation rate of 0.5 mm/min. IRLD spectra are collected at each strain point, once stretching has ended. Spectral acquisition (for the chosen resolution and number of scans collected) requires about 30 min per strain point. The Minimat is capable of performing uniaxial deformation in increments of 0.3 μm up to 10 cm total elongation (580% strain for our gauge samples). Furthermore, a custom-modified environmental chamber provides for accurate temperature control ranging from ambient conditions to 200 °C. The chamber is also equipped with potassium bromide (KBr) windows to provide thermal insulation and optical transparency for the infrared beam.

Calibration and Background Spectra. Raw IRLD spectra need to be normalized in order to obtain meaningful results. Three different pairs of calibration spectra are acquired: "aligned-polarizer" (P_B and P_D), "crossed-polarizer" (Q_B and Q_D), and "open-beam" (M_B and M_D). Aligned-polarizer spectra are acquired with a second linear polarizer—an ideal, anisotropic "sample"—placed between the PEM and the detector. Crossed-polarizer spectra are obtained by rotating the second linear polarizer ninety degrees, so that its polarization axis is perpendicular to that of the first polarizer. P_B, P_D, Q_B, and Q_D contain information about the polarization modulation efficiency of the PEM as well as the residual anisotropy of the optical train. Open-beam spectra are acquired with the second polarizer removed from the IR beam path. M_B and M_D contain information about the optical throughput of the instrument. In summary, six different spectra are obtained and used to normalize IRLD spectra.

Infrared Dichroism Background and Theory. By definition, linear dichroism is the preferential absorption of one of two mutually perpendicular components of linearly polarized (or "plane-polarized") light.[42] Thus, we have an absorbance

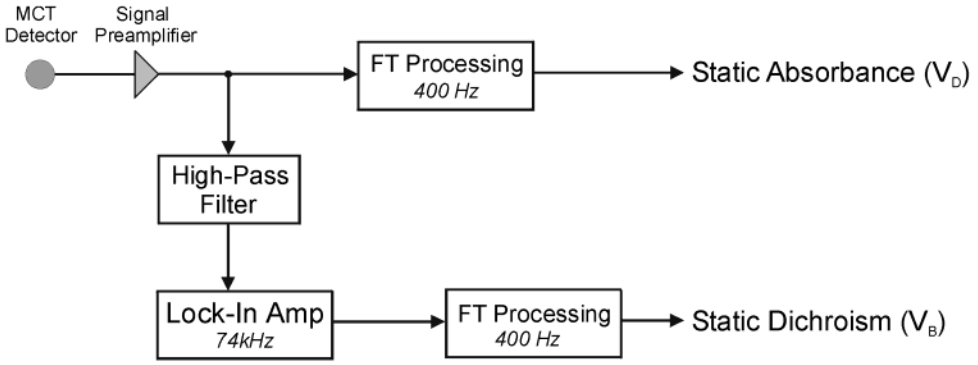

Figure 2. Schematic diagram of the rheo-FTIR signal processing to extract both raw absorbance and raw dichroism spectrum.

component of light polarized parallel to the stretching direction, $A_{\parallel}(\tilde{\nu})$, and absorbance of light polarized perpendicular to the stretch, $A_{\perp}(\tilde{\nu})$. An important parameter used to describe optically measured macromolecular orientation over the past 50 years is the dichroic ratio, defined as

$$D(\tilde{\nu}) \equiv \frac{A_{\parallel}(\tilde{\nu})}{A_{\perp}(\tilde{\nu})}$$

A mathematical relationship between D and a molecular orientation function, f, was derived by Hermans et al.[43]

$$f = \left(\frac{D-1}{D+2}\right)\left(\frac{D_{\infty}+2}{D_{\infty}-1}\right)$$

where D_{∞} is the dichroic ratio of an ideal uniaxially oriented system. More recently, the dichroic difference (or, simply, dichroism), $\Delta A(\tilde{\nu}) \equiv A_{\parallel}(\tilde{\nu}) - A_{\perp}(\tilde{\nu})$, has been used as a parameter that is more sensitive to experiments involving small changes in dichroism. With some mathematical substitution and rearranging, it may be shown that

$$f = \frac{\Delta A}{\Delta A_{\infty}}$$

where again, the infinity subscript denotes the case of perfect anisotropy. The true utility of infrared dichroism is 2-fold. First, infrared absorbance has proved sensitive to the local molecular environment of components within semicrystalline polymers. Therefore, IR dichroism can probe orientation for macromolecular chains of different conformations. When correlated with crystallographic data, IR spectra can be used to characterize crystalline, mesomorphic, and amorphous domains as well. Second, using Fourier transform IR spectroscopy and appropriate detection optics, a polychromatic light source may be used. Thus, the orientation/anisotropic responses of multiple moieties to a common perturbation may be measured simultaneously.

As a polymer film is stretched, it is assumed that the main ("backbone") chain and its associated ("skeletal") vibrational dipole moments align primarily with the direction of tensile force (hence, an intrinsic assumption that these dipoles orient along the direction of their associated chemical bonds). The orientation of side ("pendant") groups is dictated by their geometric relationships to the main chain due to covalent bonding. Thus, a chemical functionality whose vibrational dipole possesses a net orientation parallel to the applied stretch will give rise to a positive ΔA value ($\Delta A > 0$, since $A_{\parallel} > A_{\perp}$) at its characteristic IR wavenumber(s). Likewise, moieties that orient perpendicular to the stretching direction will give negative dichroism values ($A_{\perp} > A_{\parallel}$, thus $\Delta A < 0$). The general assignment of sPP vibrational moments as "parallel" or "perpendicular" has already been undertaken.[44]

Consider a tensile strain applied to a polymer film

$$\epsilon(t) = \bar{\epsilon} + \tilde{\epsilon}(t)$$

where the total strain, ϵ, may consist of a static component, $\bar{\epsilon}$, a transient component, $\tilde{\epsilon}$, or both. The polymer will respond to this mechanical perturbation by exhibiting a stress

$$\sigma(t) = \bar{\sigma} + \tilde{\sigma}(t)$$

where σ, $\bar{\sigma}$, and $\tilde{\sigma}$ are the stress analogies of the strain terms. We assert that the resultant stress will cause some molecular reorientation within the film. Thus, we may conclude that dichroism responds to the applied strain in a similar fashion.

$$\Delta A(\tilde{\nu},t) = \Delta\bar{A}(\tilde{\nu}) + \Delta\tilde{A}(\tilde{\nu},t)$$

where $\Delta\bar{A}$ and $\Delta\tilde{A}$ are the static and dynamic components of infrared linear dichroism, respectively. For experiments in the present work, the applied tensile perturbation is expressed simply as $\epsilon = \bar{\epsilon}$. Hence, $\sigma = \bar{\sigma}$ and $\Delta A = \Delta\bar{A}(\tilde{\nu})$; that is, only static components exist.

To recover the raw dichroism signal, $V_B(\tilde{\nu},\epsilon)$, the double-modulated detector signal is decoded by a lock-in amplifier referenced to the PEM. For these experiments, the detected signal contains two modulations, imposed successively by the Michelson interferometer and the PEM. The spectrometer Fourier transform processing unit then further demodulates the lock-in amplifier output signal. In a separate measurement, the raw absorbance signal, $V_D(\tilde{\nu},\epsilon)$, is obtained by demodulating the detector signal using the 400-Hz reference signal only. The absorbance measurements are unaffected by the PEM, since FT processing rejects all frequencies greater than 400 Hz. A schematic breakdown of detector signal demodulations is given as Figure 2. The static IRLD spectrum at each deformation point, $\Delta A(\tilde{\nu},\epsilon)$, is calculated according to the procedure suggested by Noda et al.[45] Signals resulting from the demodulation steps are combined with the appropriate background spectra. The parallel and perpendicular transmittances for irreversibly deformed samples are calculated by

$$T_{\parallel}(\tilde{\nu},\epsilon) = \frac{P_B(\tilde{\nu})V_D(\tilde{\nu},\epsilon) - P_D(\tilde{\nu})V_B(\tilde{\nu},\epsilon)}{P_B(\tilde{\nu})M_D(\tilde{\nu}) - P_D(\tilde{\nu})M_B(\tilde{\nu})} \quad \text{and}$$

$$T_{\perp}(\tilde{\nu},\epsilon) = \frac{Q_B(\tilde{\nu})V_D(\tilde{\nu},\epsilon) - Q_D(\tilde{\nu})V_B(\tilde{\nu},\epsilon)}{Q_B(\tilde{\nu})M_D(\tilde{\nu}) - Q_D(\tilde{\nu})M_B(\tilde{\nu})}$$

Absorbance is defined as the negative logarithm of transmittance. Thus, quantitative dichroism can be obtained as

$$\Delta A(\tilde{\nu},\epsilon) = -\log\left[\frac{T_{\parallel}(\tilde{\nu},\epsilon)}{T_{\perp}(\tilde{\nu},\epsilon)}\right]$$

Wide-Angle X-ray Diffraction (WAXD). WAXD experiments were performed at the Brookhaven National Laboratory (Upton, NY). Diffraction patterns were collected with a charge

coupled device (CCD) camera (158.44 μm pixel-to-pixel resolution) using synchrotron radiation tuned to a wavelength of 1.366 Å. An alumina (Al_2O_3) standard diffraction ring (2θ = 22.61°) was used for calibration. All raw data for polymer films are ratioed by a background scan (i.e., with no sample). Since the synchrotron source intensity is time dependent, data are further normalized by a relative overall intensity, as measured by an ion chamber prior to each sample scan. Each scan is performed once with 10 s of radiation exposure, and then repeated with 30 s of exposure. Two-dimensional diffraction patterns and corresponding one-dimensional diffractograms are reported for 30-s exposure times. To observe crystalline orientation, the 2-D patterns were scanned azimuthally and plotted. Azimuthal data are smoothed using an appropriate binomial function.

Raman Scattering. Raman spectra were collected using an unpolarized source at ≈180° (i.e., nearly backscattering mode) with an *f*/6.4 TRIAX-550 Raman spectrometer (Jobin-Yvon, Ltd.). The diffraction grating used has a groove density of 1200/mm, providing a spectral resolution slightly better than 4 cm^{-1}. The entrance slit was set to a constant width of 0.2 mm. A krypton−argon ion laser (model 165/265, Spectra Physics, Inc.) provided 400 mW of excitation at a wavelength of 514.5 nm. A liquid-nitrogen-cooled CCD detector system (Spectrum One Instruments, S.A.) is used to collect dispersed photons. Radiation counts were accumulated over an integration time of 15 s with five scans co-added. The spectrometer is calibrated using solid silicon and mercury vapor standards. If necessary, subsequently acquired sample spectra undergo a horizontal shift (wavenumber correction) equal to the difference between actual and tabulated Raman shift values for the calibration standards. SpectraMax software (Jobin-Yvon, Ltd. and Galactic Industries Corp.) is used both to compile and process data from the detector and to control spectrometer settings.

Results

We first offer a brief note concerning the strain values listed for the illustrations to follow. For WAXD and Raman data, the strain values given are those to which a given sample *has been* tensile stretched (i.e., WAXD and Raman are ex situ). For these two experiments, samples are first released from tension ("unhooked") and then remounted on an appropriate stage for analysis. The actual strain on the sample (i.e., its irreversible or "residual" component) during WAXD and Raman scans is clearly less than the strain achieved under tension, due to the partial elastic character of sPP. In contrast, strain values reported for IRLD experiments are the actual strains, since the films are under tension ("hooked" or in situ) while spectra are acquired.

Mechanical. Figure 3 shows tensile mechanical behavior for both quenched and slow-cooled material. Both materials show reversible, elastic behavior initially, up to a yield point (∼20% strain for quenched, ∼40% for slow-cooled). The quenched material continues to deform, giving a constant stress response up to 400% strain. The stiffer, morecrystalline slow-cooled material exhibits a greater elastic modulus than the quenched material (92 vs 78 MPa), and fails much earlier (∼200% strain). In the present work, tensile mechanical behavior for slow-cooled sPP is reported up to a strain of 200%, yet IRLD data is limited to 50% strain. For tensile stress−strain data, thicker samples (∼200 μm) were used since IR transmittance was not a concern.

WAXD. Elastic Region. The unstretched samples [both slow-cooled (Figure 4A) and quenched (Figure 4B)] primarily display reflections consistent with the form I crystal morph[13] (see Table 1). Because of the absence of the 211 reflection (d = 4.71 Å, 2θ = 16.66°, $2\theta_{Cu\ K\alpha}$ = 18.8°; unique to limit-ordered form I), however, the peaks are assigned to the disordered form I variant. The same assignment of the disordered form I variant is consistent throughout the other four quenched samples. As indicated in Figure 4, parts A and B, the presence of the mesophase[34] in the unstretched samples is possible. This is indicated by the presence of a broad shoulder to the right of the peak centered at 2θ = 14.07° ($2\theta_{Cu\ K\alpha}$ = 15.86°, d = 5.34 Å), indexed as the 110 and 020 planes (d = 5.21 Å, assuming an orthohexagonal unit cell and parameters a = 6.02 Å, b = 10.42 Å, and c = 5.05 Å, as in ref 30). This peak is difficult to assign, however, since form II has a peak at nearly the same angle (d = 5.22 Å) and shares other peaks in common with form I that are also present. Also, another peak at 2θ = 21.05° ($2\theta_{Cu\ K\alpha}$ = 23.74°, d = 3.74 Å) is consistent with the 101 and 111 mesophase planes (d = 3.87 and 3.63 Å, respectively) but overlaps with the 002 peak of form I (2θ = 21.13°, $2\theta_{Cu\ K\alpha}$ = 23.86°, d = 3.73 Å). This tentative assignment of mesophase content is also made for the quenched sample drawn to 50% strain (Figure 4C). For these samples that have not yet yielded, it is

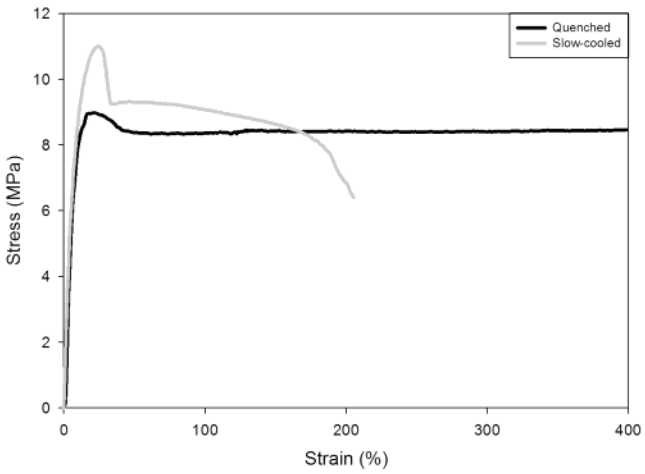

Figure 3. Tensile mechanical behavior of syndiotactic polypropylene films at room temperature (∼30 °C).

Table 1. Calculated Crystallographic Parameters for SPP Polymorphs[a]

polymorph	*hkl*	$2\theta_{hkl}$ (deg)	$2\theta_{hkl(Cu\ K\alpha)}$ (deg)	*d* (Å)
helical (forms I and II)	200[b]	10.811	12.193	7.25
	020[c]/010[d]	14.011	15.806	5.60
	211[e]	16.664	18.805	4.71
	121[c]/111[d]	18.377	20.742	4.28
	002[b]	21.131	23.859	3.73
	400[b]	21.720	24.528	3.63
form III	020	14.049	15.849	5.59
	110	16.608	18.741	4.73
	021	20.989	23.699	3.75
	111	22.803	25.755	3.46
	121	25.919	29.290	3.05
	130	26.043	29.431	3.03
mesophase	110	15.058	16.990	5.21
	020	15.066	16.998	5.21
	101	20.336	22.959	3.87
	111	21.708	24.514	3.63

[a] Bragg angles given are for synchrotron X-rays of wavelength 1.366 Å. Bragg angles for Cu Kα radiation (λ = 1.54 Å) and interplanar spacings, *d*, are also given for each *hkl* indexed plane. [b] Reflection is common to both form I and form II. [c] Reflection is indexed based on limit-ordered form I (b = 11.2 Å). [d] Reflection is indexed based on disordered form I (b = 5.6 Å). [e] Reflection is unique to limit-ordered form I (b = 11.2 Å).

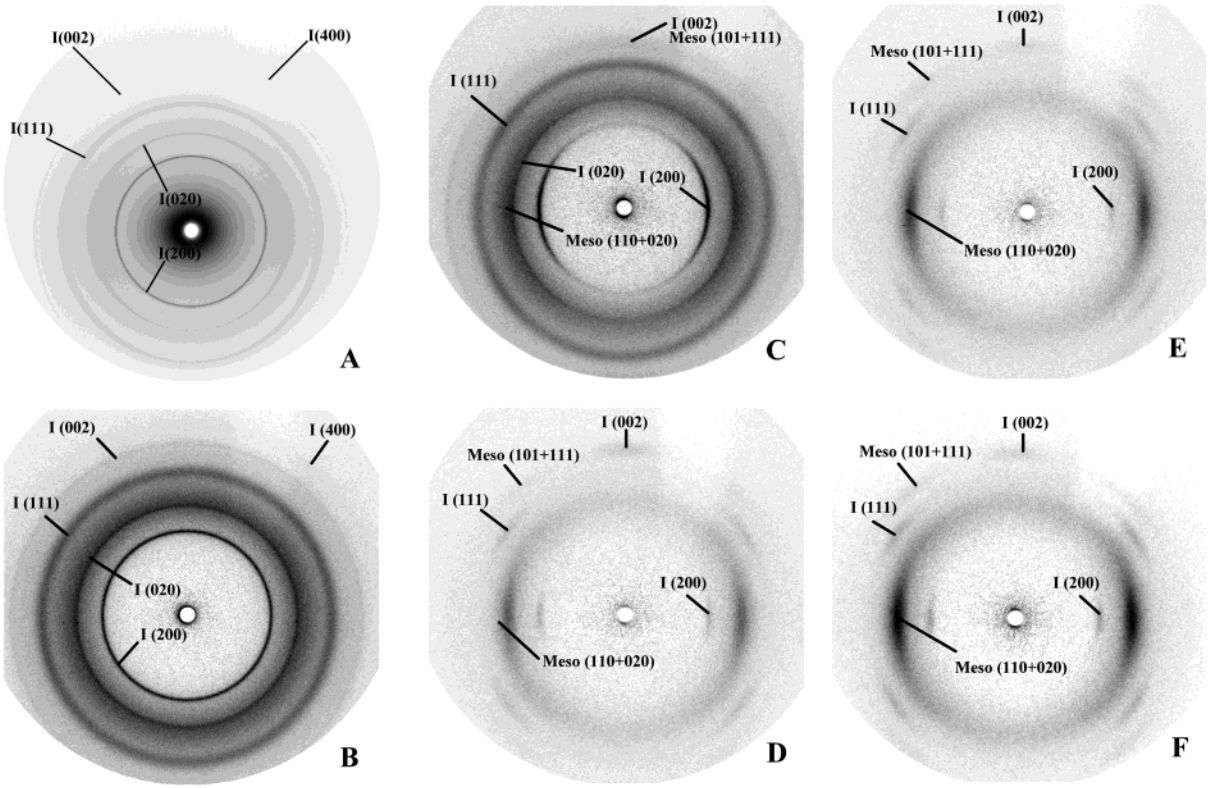

Figure 4. Ex situ 2-D WAXD patterns for (A) slow-cooled sPP (undeformed), (B) quenched sPP (undeformed), (C) quenched sPP (50% strain), (D) quenched sPP (100% strain), (E) quenched sPP (200% strain), and (F) quenched sPP (400% strain).

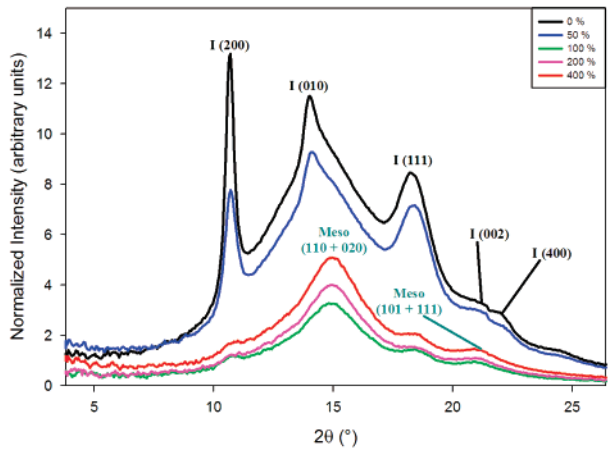

Figure 5. Ex situ WAXD diffractograms for quenched, tensile drawn sPP films.

not possible to do a layer analysis of the 2D patterns that would solidify the assignment of the mesophase, as there is not a definitive peak in the azimuthal intensity to indicate a *c* axis repeat spacing. However, in light of the findings for the samples strained beyond the yield point ($\epsilon > 50\%$), the presence of mesophase in the elastically strained sample seems more likely.

Postyield. The remaining samples, strained to 100% (Figure 4D), 200% (Figure 4E), and 400% (Figure 4F) share similar diffraction patterns that are qualitatively different from those for the previous samples. The patterns indicate the presence of the mesophase and a small amount of disordered form I. After yielding, there are four obvious peaks in the diffractograms (Figure 5); however, the 2-D patterns elucidate the presence of a fifth peak that is azimuthally centered on the meridian. These three traces show a strong, broad peak at $2\theta =$ 14.97° ($2\theta_{\text{Cu K}\alpha} = 16.88°$, $d = 5.24$ Å) that is consistent with the 110 and 020 mesophase planes (again, using the unit cell described in ref 30) and that increases in height as the sample is strained. This suggests that the relative amount of mesophase in the sample is increasing. One can discount the possibility that this peak is due to the 110 planes of form II, since the intensity is much greater than the other peaks present that might be assigned to form II. Also, the broad peak shape is inconsistent with the typically sharp diffraction peak seen at this angle for form II,[15,17,18] and it does not match the typical shape of the amorphous halo (however, we cannot verify this since we do not have a completely amorphous sample for comparison). A second peak at $2\theta = 20.9°$ ($2\theta_{\text{Cu K}\alpha} = 23.56°$, $d = 3.77$ Å) can be assigned to the 101 and 111 planes of the mesophase ($d = 3.87$ and 3.63 Å, respectively). This peak assignment is corroborated by a layer spacing of 5.05 Å, consistent with the *c* axis repeat distance for planar sPP chains in the mesophase unit cell. Coincidently, this is also the *c*-spacing for the form III unit cell, yet the pattern cannot be designated to the form III crystal morph due to the absence of diffraction peaks for the 020 ($2\theta = 14.05°$, $2\theta_{\text{Cu K}\alpha} = 15.85°$, $d = 5.59$ Å), 110 ($2\theta = 16.61°$, $2\theta_{\text{Cu K}\alpha} = 18.74°$, $d = 4.73$ Å), and 111 ($2\theta = 22.8°$, $2\theta_{\text{Cu K}\alpha} = 25.76°$, $d = 3.46$ Å) planes. Finally, the presence of a small amount of disordered form I crystals is indicated by weak peaks at $2\theta = 10.84°$ ($2\theta_{\text{Cu K}\alpha} = 12.23°$, $d = 7.23$ Å), $2\theta = 18.2°$ ($2\theta_{\text{Cu K}\alpha} = 20.54°$, $d = 4.32$ Å), and $2\theta = 20.90°$ ($2\theta_{\text{Cu K}\alpha} = 23.56°$, $d = 3.77$ Å), assigned to the 200, 111, and 002 planes, respectively. Layer analysis of the 111 (off meridian) and 002 (along the meridian) peaks gives *c* spacings of 7.38 and 7.6 Å, respectively, consistent with the form I unit cell parameter, $c = 7.45$ Å.

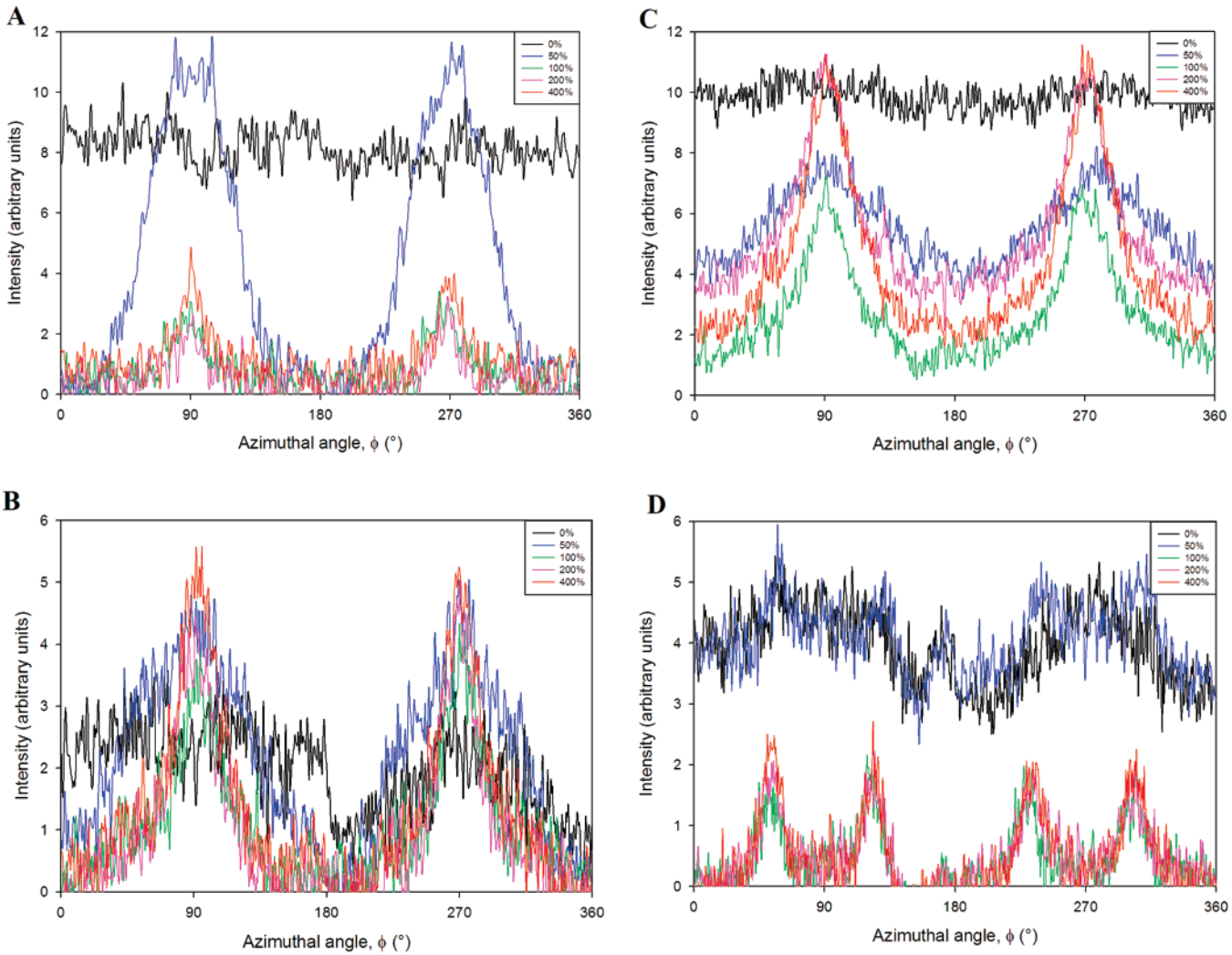

Figure 6. Ex situ WAXD azimuthal plots for syndiotactic polypropylene. Intensity at $\phi = 90, 270°$ corresponds to orientation parallel to the strain direction. Key: (A) $2\theta = 10.69°$, corresponding to the 200 plane of disordered form I; (B) $2\theta = 14.04°$, corresponding to the 010 plane of disordered crystalline form I; (C) $2\theta = 14.97°$, corresponding to the 110 and 020 planes of the paracrystalline mesophase; (D) $2\theta = 18.33°$, corresponding to the 111 plane of disordered form I.

Azimuthal Plots. One-dimensional azimuthal plots (Figure 6) show how both disordered form I crystals (Figure 6A−C) and the mesomorphic form (Figure 6D) orient with strain and remain oriented even when unhooked. Initially, unstrained films show isotropic orientation ($I(\phi)$ constant). Then, as films are tensile stretched, orientation anisotropy results, corresponding to intensity peaks at certain azimuthal angles. By convention, azimuthal intensity at $\phi = 90$ and 270° corresponds to orientation parallel to the strain axis. Thus, as might be expected, the 200 (Figure 6A) and 010 (Figure 6B) planes of disordered form I and the 110 and 020 planes of the mesophase (Figure 6C), which are all parallel to the chain axis (c axis), orient along the direction of strain ($\phi = 90, 270°$). Likewise, the 111 planes of form I (Figure 6D) show azimuthal peaks at angles of ±45° with respect to the strain direction ($\phi = 45, 135, 225, 315°$), as expected. Orientation of the sPP polymorphs will be illustrated again in IR linear dichroism spectra.

Rheo-FTIR. As stated previously, orientation for crystalline, mesomorphic, and amorphous domains can be measured quantitatively and simultaneously with linear dichroism experiment using rheo-FTIR spectroscopy. Figure 7 shows an infrared absorbance spectrum for an undeformed, quenched sPP film. Monitoring IR

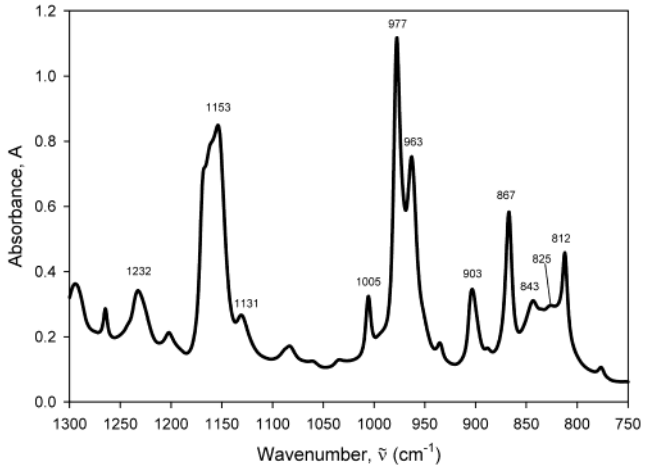

Figure 7. Infrared absorbance spectrum of an undeformed syndiotactic polypropylene film prepared via quenching from the melt and subsequent annealing at room temperature. The spectrum was acquired in rapid-scan mode at room temperature (~30 °C) with a resolution of 1 cm^{-1} and 10 000 scans co-added.

Table 2. Conformation-Sensitive Infrared Absorbance Peaks for Syndiotactic Polypropylene[a]

wavenumber (cm^{-1})	conformation assignment	morphology assignment
812	helical	form I
825 (absorbance)	planar	amorphous
838 (dichroism)	helical and planar (825 + 843 contributions)	amorphous
843 (absorbance)	helical	amorphous
867	helical	form I
903	helical	form I
949	planar	mesophase or form III (?)
963	planar	mesophase and amorphous
977	helical	amorphous
1005	helical	form I
1131	planar	amorphous
1153	conformation insensitive	amorphous
1232	planar	amorphous

[a] For each peak wavenumber are listed any molecular chain conformations or crystalline structures represented by the peak.

absorption peaks during deformation provides insights into the changes in relative amounts of helical and planar chains, as well as crystalline or amorphous content. IR dichroism peaks provide insights into the orientation responses of each type of chain conformation and morphology. A list of characteristic IR peaks for sPP and the structural assignments are given in Table 2.[44,46,47]

IR Absorbance. Absorbance spectra as a function of tensile strain are given in Figure 8. For the unstrained quenched sample (Figure 8A), peaks characteristic of helical chain conformation are predominant ($\tilde{\nu}$ = 812, 843, 867, 903, 977, 1005 cm^{-1}). A parameter commonly used to measure the overall relative helical-to-planar content of sPP is the absorbance ratio A(977 cm^{-1})/A(963 cm^{-1}).[48] The value of this parameter vs tensile strain is given in Figure 9. Below 25% strain, the ratio is relatively constant for both quenched and slow-cooled samples. As expected, the slow-cooled sample exhibits a higher helical-to-planar ratio than the quenched sample, since form I crystal growth is encouraged at higher temperatures. As sPP films begin to undergo yielding (ϵ > 25%), helical content begins to decrease. At strains greater than 50%, IR peaks representing both planar and amorphous chains are dominant ($\tilde{\nu}$ = 825, 963, 1131, 1232 cm^{-1}). Upon yielding, certain helical peaks almost disappear ($\tilde{\nu}$ = 812, 843, 1005 cm^{-1}), while others are still present to a lesser extent ($\tilde{\nu}$ = 867, 903, 977 cm^{-1}). This is because, even at the highest strains, sPP chains in helical sequence may not be completely eliminated. At the greatest strains ($\epsilon \geq$ 300%), a small absorbance peak emerges at $\tilde{\nu}$ = 949 cm^{-1}. On the basis of the sharpness of the peak and its relatively large dichroism response at highest strains, we suggest that it may be indicative of form III crystallites. (Recall that IR data is acquired in situ, whereas WAXD patterns, which show no evidence of form III, are collected for relaxed films.) In summary, for quenched sPP, there is a gradual strain-induced transformation in overall chain conformation from helical to planar over the range of strains investigated. We see the gradual disappearance of form I crystals (as supported by WAXD) but not the complete disappearance of helical chains.

IR Dichroism. IRLD spectra for quenched and slow-cooled samples are given in Figure 10, parts A and B, respectively. Although steps were taken to form sample

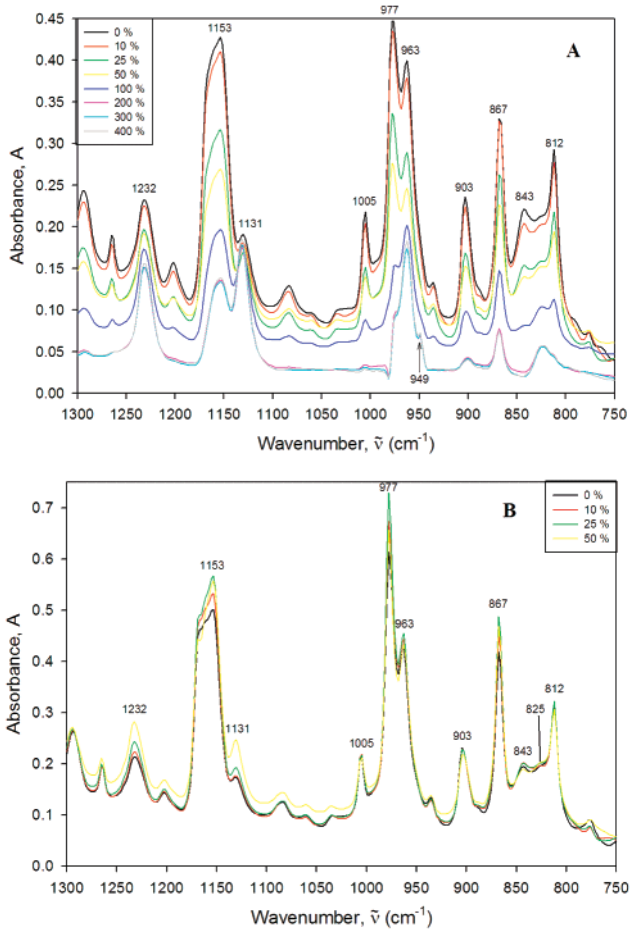

Figure 8. In situ IR absorbance spectra for (A) quenched sPP and (B) slow-cooled sPP films tensile deformed to various strain points. Spectra are acquired in step-scan mode at room temperature (~30 °C) with a resolution of 4 cm^{-1} and 32 scans co-added. Vertical offset between traces is due to thickness changes incurred from tensile stretching.

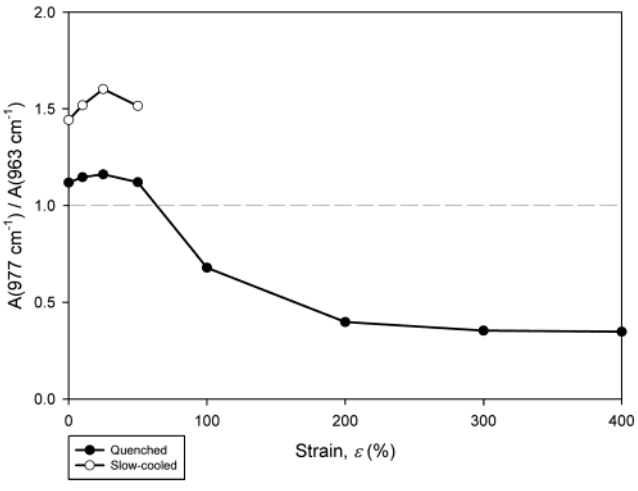

Figure 9. In situ absorbance ratio of 977 and 963 cm^{-1} peaks for sPP as a function of tensile strain. This parameter quantifies relative helical and planar chain conformational content.

films with no net orientation, some anisotropy is present for both unstrained quenched and slow-cooled samples, as evidenced by small, nonzero dichroism peaks at 812, 867, 963, and 977 cm^{-1}. Loos and Petermann cite the ability of lamellae in semicrystalline polypropylene to orient preferentially as a function of crystallization

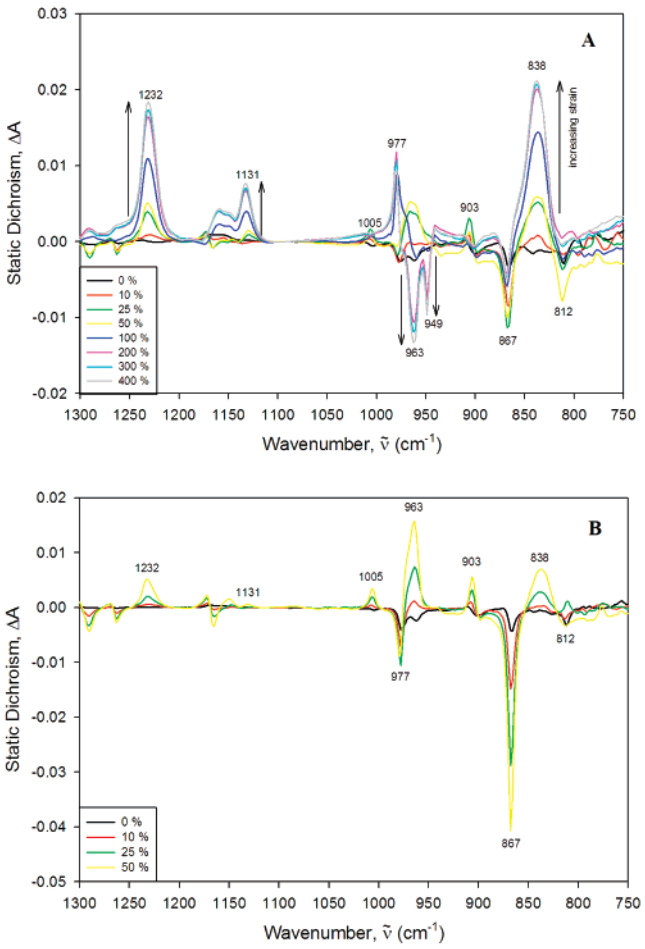

Figure 10. In situ IRLD spectra for (A) quenched sPP and (B) slow-cooled sPP films tensile deformed to various strain points. Spectra are acquired in step-scan mode at room temperature (~30 °C) with a resolution of 4 cm^{-1} and 32 scans co-added. Vertical arrows indicate the direction of magnitude change for certain peaks as strain increases.

temperature.[49] This initial dichroism signal may also be a response to some small strain applied while mounting the sample between stretcher jaws.

For tensile strains up to the yield point (≤50%), form I crystals show a gradual, increasing orientation response with strain in quenched samples (812, 867, 903, and 1005 cm^{-1} increase in magnitude). Dichroism peaks for slow-cooled samples in this strain region behave almost identically to those for quenched samples. Of course, the more crystalline slow-cooled sample gives an orientation response of greater magnitude for form I peaks. It is interesting to note that for all strains, peaks sensitive to both planar and amorphous chains show increasing dichroism responses at very similar rates ($\tilde{\nu}$ = 1131, 1232 cm^{-1}). A broad dichroism peak, centered at $\tilde{\nu}$ = 838 cm^{-1} exhibits the dichroism response of greatest magnitude. ΔA(838 cm^{-1}) behaves in a manner very similar to ΔA(1131 cm^{-1}) and ΔA(1232 cm^{-1}), its magnitude increasing in the same direction and at a similar rate. By correlating the behaviors of absorbance and dichroism spectra in the region $\tilde{\nu}$ = 850−820 cm^{-1}, we assign the 825 and 843 cm^{-1} peaks (observed in absorbance spectra) to planar and helical conformations, respectively. Furthermore, the relatively large magnitude and width of ΔA(838 cm^{-1}), in addition to its behavior as the quenched film is tensile deformed, suggests that it is representative of the amorphous domain and is composed of contributions from both helical (843 cm^{-1}) and planar (825 cm^{-1}) chains.

Upon yielding ($\epsilon \geq 100\%$), the IRLD spectrum for quenched sPP undergoes marked changes:

1. Helical peaks show an abrupt decrease in magnitude. Likewise, the magnitudes of planar dichroism peaks increase.

2. The amorphous domain response to strain increases suddenly.

3. Some dichroism peaks undergo a "flip" (i.e., 963 and 977 cm^{-1} change sign from negative to positive or vice versa). Physically, a dichroism peak flip represents a change in the overall orientation direction of a given moiety.

Magnitude changes in dichroism peaks are caused by one of two events:

1. The amount of a certain morphology present in the sample has changed.

2. The extent to which a given moiety orients has changed.

The magnitude decrease for helical peaks sensitive to form I is most likely due to the sharp decrease in helical chain content upon yielding (as evidenced by IR absorbance) and not to a decrease in orientation (as also supported by WAXD azimuthal plots). When the sample yields, the orientation of form I crystallites reaches a maximum.

As mentioned above, we assert that ΔA(838 cm^{-1}) is sensitive to both helical and planar amorphous chains. This peak assignment is in good agreement with our proposed mechanism of physical deformation in quenched sPP. Upon yielding, the 838, 1131, and 1232 cm^{-1} dichroism peaks show a remarkable increases in magnitude: first, from 50 to 100% strain, and again from 100 to 200% strain. We suggest that these jumps in ΔA magnitude are due to two factors:

1. First is the fact that the noncrystalline domain must bear any strain applied after the crystalline domain yields. This clearly demonstrates the sensitivity of 838 (825 + 845 cm^{-1}), 1131, and 1232 cm^{-1} to amorphous domain anisotropy. This physical model also explains the magnitude jump and peak flip of ΔA(977 cm^{-1}). This peak is sensitive to the orientation of helical chains in noncrystalline regions. Prior to yielding, the orientation of the noncrystalline helical chains is understandably low, since form I crystals give the greatest response to applied strain in this region. form I crystals begin to break up with continued strain. Of the helical chains that once composed form I crystals, the majority undergoes a conformation change into planar chains. The remnant, however, retains its helical conformation, resides in the amorphous domain, and orients along with the rest of the amorphous chains [ΔA(977 cm^{-1}, $\epsilon \geq 100\%$) is positive]. It is interesting to see that ΔA(977 cm^{-1}) reaches a maximum value at ϵ = 200% and decreases slightly at higher strains. This decrease in orientation response is probably due to the ongoing strain-induced conformation change in helical chains. The presence of helical chains in sPP, even at high strains, has been observed previously.[30,35]

2. Highly oriented planar chains begin to compose the paracrystalline mesophase. This explains the peak flip and magnitude change of the 963 cm^{-1} dichroism peak. While 963 cm^{-1} is characterized similarly to 1131 and 1232 cm^{-1} in the literature[46] (i.e., sensitive to both planar chains and amorphous content), its dichroism behavior is unique. Prior to yielding, ΔA(963 cm^{-1}) is a

broad, positive peak whose magnitude increases with strain. After the film yields, $\Delta A(963\ cm^{-1})$ is nearly zero at 100% strain, and becomes a sharp, strong, negative peak at 200% strain. Unlike $\Delta A(977\ cm^{-1})$, which also flips after yielding, $\Delta A(963\ cm^{-1})$ continues to increase in magnitude up to 400% strain. From 100 to 400% strain, WAXD data confirms the increasing formation and orientation of the mesophase. This correlation suggests that the 963 cm^{-1} peak is highly sensitive to the orientation of planar chains in the mesophase at high strains.

At the highest strains, a strong, very sharp, negative dichroism peak emerges at 949 cm^{-1}. At this point, we cannot be certain whether 949 cm^{-1} is due to the mesophase or the presence of form III crystals (again, this is because WAXD data are acquired ex situ). In light of this, we offer some attributes of this peak in support of its assignment as characteristic of form III:

1. Relative to other absorbance and dichroism peaks, $A(949\ cm^{-1})$ and $\Delta A(949\ cm^{-1})$ are "sharp" (i.e., narrow, with a precise maximum). Sharp, well-defined peaks commonly represent regular, ordered structures in all types of spectroscopic methods.

2. The peak only appears at higher strains. We know from the literature that form III crystals appear while melt-quenched sPP is under appreciable tensile strain (≥400%).[30,35] Perhaps, we are observing the initial stages of form III crystallite growth.

3. $\Delta A(949\ cm^{-1})$ points in the same direction as $\Delta A(963\ cm^{-1})$. It is intuitive to assume that form III crystals will possess an orientation similar to that found in their early stages of formation.

Raman Scattering. Raman spectra are presented in Figure 11. Hsu et al. have found certain Raman scattering peaks to be sensitive not only to sPP chain conformations,[50] but also to configurational (stereoregularity) defects.[51] These are listed in Table 3. A prominent peak at 310 cm^{-1} is indicative of high syndiotactic content in each sample. Of greater interest are three adjacent peaks at 823, 845, and 867 cm^{-1}. These Raman shifts are characteristic of helical chains, amorphous content, and planar chains, respectively. While the spectra illustrated in Figure 11A contain many peaks, the present work will focus on changes to the aforementioned trio with applied tensile strain. To account for differences in film thickness from sample to sample, each spectrum has been ratioed with the intensity of its respective 1153 cm^{-1} peak. This peak, insensitive to sPP chain conformation, is an ideal candidate to help provide normalized, quantitative data (Figure 11B).

It is readily apparent that the Raman data are in good agreement with the other results reported. Quenched samples initially possess a greater amount of helical chains (823 cm^{-1}) than planar chains (867 cm^{-1}). As the quenched sample undergoes tensile strain, the relative planar content increases, eventually exceeding helical content at 100% strain. It must be noted that the existence of form I and form III crystallites cannot be inferred exclusively from the presence of helical and planar peaks, respectively. This conclusion can only be made using data resulting from a crystallographic experimental method. However, Raman spectra do illustrate the relative amounts of different sPP chain conformations.

The spectrum at 100% strain (Figure 11B) shows characteristic helical and planar peaks that are slightly shifted to lower wavenumbers. Hsu et al. explain that

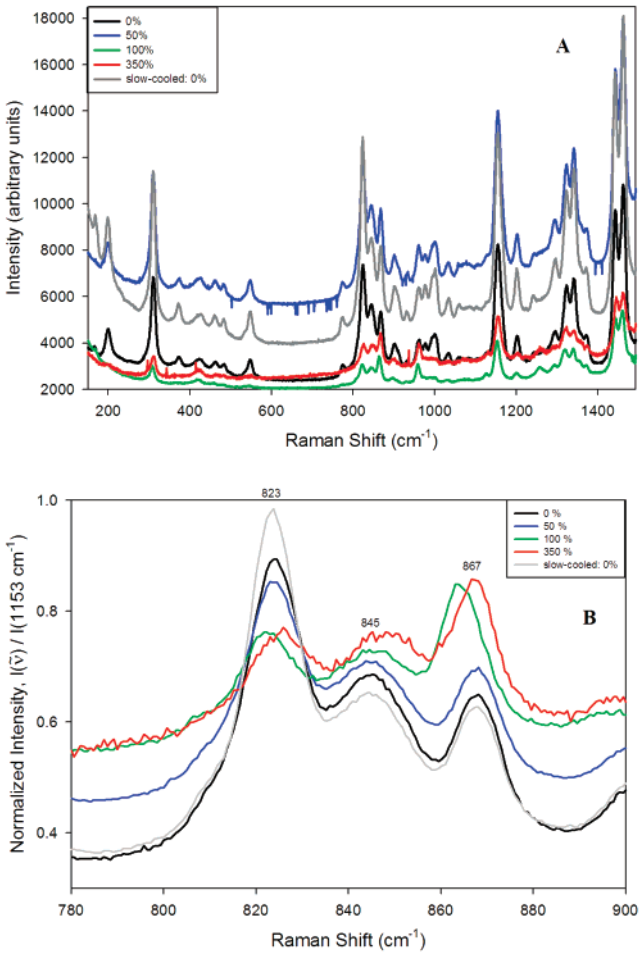

Figure 11. Ex situ Raman scattering spectra for syndiotactic polypropylene acquired at room temperature (~30 °C). Key: (A) total intensity vs Raman shift; (B) normalized plots of specific peaks sensitive to sPP molecular chain conformation.

Table 3. Conformation- and Configuration-sensitive Raman Scattering Peaks for Syndiotactic Polypropylene

Raman shift (cm^{-1})	assignment
310	syndiotacticity index: varies from 290 to 310 based on syndiotactic content
823	helical $(ggtt)_n$ conformation
845	amorphous
867	trans-planar $(tttt)_n$ conformation

each characteristic Raman peak for propylene, whether syndiotactic or isotactic, may appear within a small range of wavenumbers (about 20 cm^{-1}).[51] The exact position at which the peak appears is influenced by the presence of any defects in chain conformation. In general, peaks at greater shift values are due to chains possessing greater conformational order (i.e., fewer defects). This supports a physical model where sPP chains are in transition from helical to planar conformation. This transitional state consists of molecular chains possessing shorter sequences of their respective conformations. As a tensile-strain-induced conversion of chains occurs, long helical sequences are interrupted and new planar sequences begin to grow. The overall decrease in sequence length for both chain conformations is reflected in their respective Raman peaks shifting to lower wavenumbers. Upon completion of this transformation at higher strains ($\epsilon = 350\%$), the characteristic peaks for both helical and planar chains return to their long-sequence limiting values. A normal-

ized scattering trace is also given in Figure 11B for an undeformed slow-cooled film, rich in form I crystallites, and hence, helical chains. As expected, the scattered intensity at 823 cm^{-1} is much greater than at 867 cm^{-1} for this sample.

Discussion

Our data suggest the following picture for the physical deformation behavior of highly syndiotactic polypropylene. Initially, samples that are melt-quenched and subsequently annealed at room temperature contain form I crystals and noncrystalline chains of both helical and planar conformation. As films are stretched in the elastic region, form I crystals respond strongly to the applied strain. This is evidenced in rheo-FTIR dichroism spectra and WAXD azimuthal plots. IRLD spectra show that slow-cooled films behave similarly to quenched films in this strain range. At some point after 50% strain, the quenched film yields, and two changes in overall morphology are set into motion. Form I crystallites begin to break up into shorter helical segments, all the while retaining their overall orientation. Simultaneously, many helical chains experience a transformation into a planar conformation. Such a breakup of form I lamellae was seen by Komoto et al. in TEM micrographs.[52] The resulting helical chains are too small to form regular crystallites. Horizontal wavenumber shifts in Raman spectra illustrate the helical-to-planar conformation change very well. WAXD diffractograms and IR absorbance spectra also show the disappearance of form I in a clear manner. Furthermore, the increased orientation response of the amorphous domain—a result of form I crystal yielding—is seen clearly for IRLD spectra at strains above 50%. As strain continues to increase, planar chains begin to aggregate into a partially disordered, paracrystalline region (or, "mesophase").[34] This appears as a moderately broad WAXD peak at $2\theta = 14.97°$ and is the dominant feature in diffractograms for strains above 50%. Up to 400% strain, planar chains in the mesophase and amorphous domains continue to show greater orientation, while noncrystalline helical content decreases slightly.

As our measurements include tensile strain values only up to 400%, our results, at present, cannot be definitive with regards to the two currently existing, but contrasting mechanisms of deformation in sPP, which resulted from previous work where sample films were stretched to 700% strain and subsequently relaxed.[21,22,28−30,34] Recent works by Guadagno et al.[28−30] give insight regarding how sPP morphology would change if our quenched sample films were stretched beyond 400% strain. As fibers are drawn beyond 400% strain, the mesophase continues to increase in overall orderliness until it has completely transformed into crystalline form III. Simply removing tension was found to reverse this step; form III crystals transform back into the mesophase. Some helical chains also appear upon sample relaxation. This semiordered state is depicted as consisting of planar-rich mesomorphic domains connected by partially ordered, intercrystalline (helical) amorphous chains. Guadagno et al. state that while it is necessary for the helical-to-planar transformation to pass through a mesomorphic state, it is not clear whether such an intermediate state is traversed during the mesophase-to-form III change. Furthermore, the authors speculate the role of the mesophase on elastomeric behavior in a recent work.[30] Analogous studies have been performed for melt-crystallized and melt-slow-cooled sPPs, initially very rich in form I, by De Rosa et al.[22,34] and Auriemma et al.[21] Similar to melt-quenched films, slowly cooled samples undergo a chain conformation transition from helical to trans-planar when tensile strained. Upon relaxation, however, these films, initially rich in disordered form I crystals, adopt primarily the form II morphology. Thus, our results do agree to an extent with both of the currently proposed sPP deformation mechanisms. Up to tensile strains of 400%, the orientation and conformation changes of sPP chains can be observed clearly. However, strain/thickness limitations keep us from exploring higher strain values and obtaining comparable results (i.e., up to 700% strain) using the rheo-FTIR apparatus.

Conclusion

Our results on the deformation-induced morphology changes in sPP films, as investigated using WAXD, rheo-FTIR, and Raman spectroscopy, illustrate the utility of the rheo-FTIR technique in measuring complex orientation behavior. Tensile-strain-induced changes in morphology of highly syndiotactic polypropylene (sPP) have been investigated using optical and mechanical methods. Samples quenched from the melt and subsequently annealed at room temperature initially contain molecular chains of both $(ggtt)_n$ helical and all-trans, $(tttt)_n$, planar conformations. Samples left to cool slowly from the melted state are initially rich in helical chains and the highly stable form I crystalline polymorph. For melt-quenched films, we observe a gradual morphology transformation from the helical form I phase to a mesophase as they endure tensile deformation up to 400% strain at room temperature. The mesophase appears to be a stable interfacial region where macromolecular chains undergo conformational changes as tensile strain is applied. Ex situ wide-angle X-ray diffraction (WAXD) and in situ rheo-FTIR spectroscopy confirm the presence of form I crystallites in both undeformed quenched and slow-cooled samples. As samples are tensile strained, WAXD diffractogram peaks characteristic of form I helices gradually disappear and are eventually replaced by a single broad peak at $2\theta = 14.97°$, suggesting the presence of a mesophase rich in molecular chains of the trans-planar conformation. Previous studies show that tensile strain beyond 400% eventually causes the formation of crystalline form III. This might be characterized by the appearance of an as-yet unassigned infrared peak at 949 cm^{-1}.

Ex situ Raman spectra are in good agreement overall with the proposed transformation scenario. Raman peaks sensitive to helical and planar chain sequences change their relative peak heights accordingly. As tensile strain is applied, the planar 867 cm^{-1} peak increases relative to the helical 823 cm^{-1} peak. Over the course of this strain-induced morphology change, the most severe change in all experimental data occurs between the 50% and 100% strain points. It is at this stage that the sample film yields, and we observe a large amount of sPP chains to undergo a helical-to-planar conformation change. A momentary shift to lower wavenumbers, as seen in the Raman spectrum for the quenched sample strained to 100%, provides evidence of a reduction in overall sequence length for both conformations—simultaneous helical sequence interruption and planar sequence growth as chains transform from one conformation to another.

Infrared absorbance also gives evidence of changing sPP conformations with tensile strain. Peaks sensitive to helical sequences decrease gradually with strain while planar peaks show a concurrent increase in relative intensity. Infrared dichroism spectra provide information regarding the overall orientation of crystalline, mesomorphic, and amorphous domains with strain. Both quenched and slow-cooled films show similar dichroism responses for strains up to 50%. At these strains, form I helices and amorphous domains show a steady, monotonic increase with strain. While slow-cooled samples fail shortly after this point, quenched samples continue to undergo conformational change. Upon yielding, dichroism peaks sensitive to amorphous helical and mesomorphic planar chains experience a flip (i.e., a sign change), corresponding to the formation and orientation of the mesophase and noncrystalline helices generated from the breakup of form I crystallites. The orientation response of planar chains also increases sharply at this point. Previous work has shown that as quenched sPP samples exceed strains of 400%, they experience a reversible transition from the mesophase to crystalline form III. The present work has characterized the morphological and orientational dynamics of melt-quenched sPP thin films as they are tensile deformed up to this point.

Acknowledgment. We thank Professor Vaman Naik of the Wayne State University Electrical and Computer Engineering Department for assistance in performing Raman scattering experiments. We thank Professors Julia Kornfield (Caltech) and Stephen Z. D. Cheng (U. Akron) for valuable discussions. We also thank Dr. Shivshankar Venkataramani of the 3M Corp. for providing GPC analysis. Finally, we gratefully recognize funding from NSF−CAREER (DMR 9876221) (R.M.K.), NSF−IGERT (M.S.S.), and the Wayne State University Institute for Manufacturing Research (G.P.).

References and Notes

(1) Ewen, J. A.; Jones, R. L.; Razavi, A. *J. Am. Chem. Soc.* **1988**, *110*, 6255−6256.
(2) Longo, P.; Proto, A.; Grassi, A.; Ammendola, P. *Macromolecules* **1991**, *24*, 4624−4625.
(3) Grisi, F.; Longo, P.; Zambelli, A.; Ewen, J. A. *J. Mol. Catal. A, Chem.* **1999**, *140*, 225−233.
(4) Uehara, H.; Yamazaki, Y.; Kanamoto, T. *Polymer* **1996**, *37*, 57−64.
(5) Eckstein, A.; Suhm, J.; Friedrich, C.; Maier, R.-D.; Sassmannshausen, J.; Bochmann, M.; Mülhaupt, R. *Macromoleucles* **1998**, *31*, 1335−1340.
(6) Haftka, S.; Könnecke, K. *J. Macromol. Sci.—Phys.* **1991**, *B30*, 319−334.
(7) Silvestri, R.; Sgarzi, P. *Polymer* **1998**, *39*, 5871−5876.
(8) Gorrasi, G.; Vittoria, V.; Longo, P. *J. Appl. Polym. Sci.* **2001**, *80*, 539−545.
(9) Hatanaka, T.; Mori, H.; Terano, M. *Polym. Degrad. Stab.* **1999**, *64*, 313−319.
(10) Kato, M.; Tsuruta, A.; Kuroda, S.; Osawa, Z. *Polym. Degrad. Stab.* **2000**, *67*, 1−5.
(11) Lotz, B.; Lovinger, A. J.; Cais, R. E. *Macromolecules* **1988**, *21*, 2375−2382.
(12) Lovinger, A. J.; Lotz, B.; Davis, D. D. *Polymer* **1990**, *31*, 2253−2259.
(13) Lovinger, A. J.; Lotz, B.; Davis, D. D.; Padden, F. J., Jr. *Macromolecules* **1993**, *26*, 3494−3503.
(14) Lovinger, A. J.; Davis, D. D.; Lotz, B. *Macromolecules* **1991**, *24*, 552−560.
(15) De Rosa, C.; Corradini, P. *Macromolecules* **1993**, *26*, 5711−5718.
(16) De Rosa, C.; Auriemma, F.; Vinti, V. *Macromolecules* **1997**, *30*, 4137−4146.
(17) Auriemma, F.; De Rosa, C.; Ruiz de Ballesteros, O.; Corradini, P. *Macromolecules* **1997**, *30*, 6586−6591.
(18) De Rosa, C.; Auriemma, F.; Vinti, V. *Macromolecules* **1998**, *31*, 7430−7435.
(19) Auriemma, F.; Born, R.; Spiess, H. W.; De Rosa, C.; Corradini, P. *Macromolecules* **1995**, *28*, 6902−6910.
(20) Zhang, J.; Yang, D.; Thierry, A.; Wittmann, J. C.; Lotz, B. *Macromolecules* **2001**, *34*, 6261−6267.
(21) Auriemma, F.; Ruiz de Ballesteros, O.; De Rosa, C. *Macromolecules* **2001**, *34*, 4485−4491.
(22) De Rosa, C.; Gargiulo, M. C.; Auriemma, F.; Ruiz de Ballesteros, O.; Razavi, A. *Macromolecules* **2002**, *35*, 9083−9095.
(23) Natta, G.; Corradini, P.; Ganis, P. *Makromol. Chem.* **1960**, *39*, 238−242.
(24) Natta, G.; Peraldo, M.; Allegra, G. *Makromol. Chem.* **1964**, *75*, 215−216.
(25) Chatani, Y.; Maruyama, H.; Noguchi, K.; Asanuma, T.; Shiomura, T. *J. Polym. Sci., Part C: Polym. Lett.* **1990**, *28*, 393−398.
(26) Loos, J.; Hückert, A.; Petermann, J. *Colloid Polym. Sci.* **1996**, *274*, 1006−1011.
(27) Schwarz, I.; Stranz, M.; Bonnet, M.; Petermann, J. *Colloid Polym. Sci.* **2001**, *279*, 506−512.
(28) Guadagno, L.; D'Aniello, C.; Naddeo, C.; Vittoria, V. *Macromolecules* **2000**, *33*, 6023−6030.
(29) Guadagno, L.; D'Aniello, C.; Naddeo, C.; Vittoria, V. *Macromolecules* **2001**, *34*, 2512−2521.
(30) Guadagno, L.; D'Aniello, C.; Naddeo, C.; Vittoria, V.; Meille, S. V. *Macromolecules* **2002**, *35*, 3921−3927.
(31) Loos, J.; Schimanski, T. *Polym. Eng. Sci.* **2000**, *40*, 567−572.
(32) Nakaoki, T.; Ohira, Y.; Hayashi, H.; Horii, F. *Macromolecules* **1998**, *31*, 2705−2706.
(33) Ohira, Y.; Horii, F.; Nakaoki, T. *Macromolecules* **2000**, *33*, 1801−1806.
(34) Vittoria, V.; Guadagno, L.; Comotti, A.; Simonutti, R.; Auriemma, F.; De Rosa, C. *Macromolecules* **2000**, *33*, 6200−6204.
(35) Chatani, Y.; Maruyama, H.; Asanuma, T.; Shiomura, T. *J. Polym. Sci., Polym. Phys. Ed.* **1991**, *29*, 1649.
(36) Auriemma, F.; De Rosa, C.; Ruiz de Ballesteros, O.; Vinti, V.; Corradini, P. *J. Polym. Sci., Part B: Polym. Phys.* **1998**, *36*, 395−402.
(37) Siedle, A. R. The Nature of Semi-Syndiotactic Polypropylene. Sept 12, 2000, unpublished work.
(38) Men, Y.; Strobl, G. *Polymer* **2002**, *43*, 2761−2768.
(39) Hofmann, G. R.; Sevegney, M. S.; Kannan, R. M. Submitted to *Int. J. Polym. Anal. Charact.* 2003.
(40) Johnson, S. J.; Frattini, P. L.; Fuller, G. G. *J. Colloid Interface Sci.* **1985**, *104*, 440−455.
(41) Individual wavelengths within the polychromatic source are amplitude modulated at so-called "Fourier frequencies", $f = 2v\tilde{\nu}$, where v is the constant velocity of the interferometer moving mirror and $\tilde{\nu}$ is the electromagnetic wavenumber.
(42) Hecht, E. *Optics*, 3rd ed.; Addison-Wesley Longman: Reading, MA, 1998; p 327.
(43) Hermans, J. J.; Hermans, P. H.; Vermaas, D.; Weidinger, A. *Recl. Trav. Chim. Pays-Bas* **1946**, *65*, 427−447.
(44) Schachtschneider, J. H.; Snyder, R. G. *Spectrochim. Acta* **1965**, *21*, 1527−1542.
(45) Noda, I.; Dowrey, A. E.; Marcott, C. *Appl. Spectrosc.* **1988**, *42*, 203-216.
(46) Peraldo, M.; Cambini, M. *Spectrochim. Acta* **1965**, *21*, 1509−1525.
(47) Koenig, J. L.; Wolfram, L. E.; Grasselli, J. G. *Spectrochim. Acta* **1966**, *22*, 1233−1242.
(48) Guadagno, L.; D'Arienzo, L.; Vittoria, V. *Macromol. Chem. Phys.* **2000**, *201*, 246−250.
(49) Loos, J.; Petermann, J. *Polymer* **1996**, *37*, 4417−4420.
(50) Hahn, T.; Suen, W.; Kang, S.; Hsu, S. L.; Stidham, H. D.; Siedle, A. R. *Polymer* **2001**, *42*, 5813−5822.
(51) Hsu, S. L.; Hahn, T.; Suen, W.; Kang, S.; Stidham, H. D.; Siedle, A. R. *Macromolecules* **2001**, *34*, 3376−3383.
(52) Harasawa, J.; Uehara, H.; Yamanobe, T.; Komoto, T.; Terano, M. *J. Mol. Struct.* **2002**, *610*, 133−142.

MA025774+